EXCELLENT PUBLISHERS

International Journal of Current Research and Academic Review

ISSN: 2347-3215 Volume 3 Number 3 (March-2015) pp. 110-129

www.ijcrar.com

Spectroscopic and theoretical studies of 4-chloro-3-formyl-6-methylcourmarin (4C3F6MC)

R.K.Raj[1,5]*, S.Gunasekaran[2], T.Gnanasambandan[3] and S.Seshadri[4]

[1]Department of Physics, SCSVMV University, Enathur, Kanchipuram-631561, India
[2]Research & Development, St.Peter's University, Avadi, Chennai -600 054, India
[3]Department of Physics, Pallavan College of Engineering, Kanchipuram -631 502, India
[4]Department of Physics, L.N.Govt.Arts College, Ponneri-601204 India
[5]Departmet of Physics, Pachaiyappa's College for Men, Kanchipuram -631 503, India
Corresponding author

KEYWORDS

FTIR,
FT-Raman,
DFT,
MEP,
NBO,
NLO

A B S T R A C T

In this work, we report a combined experimental and theoretical study on molecular structure, vibrational spectra and NBO analysis of 4-chloro-3-formyl-6-methylcourmarin (4C3F6MC). The FT-IR (400–4000 cm^{-1}) and FTRaman spectra (100–3500 cm^{-1}) of 4C3F6MC were recorded. The molecular geometry, harmonic vibrational frequencies and bonding features of 4C3F6MC in the ground state have been calculated by using the density functional B3LYP method with 6-31G(d,p) and 6-311++G (d,p) as basis sets. The energy and oscillator strength calculated by Time-Dependent Density Functional Theory (TD-DFT) result complements with the experimental findings. The calculated HOMO and LUMO energies show that charge transfer occurs within the molecule. Finally the calculation results were applied to simulate infrared and Raman spectra of the title compound which show good agreement with the observed spectra.

Introduction

Coumarin was first synthesized in 1868. It is used in the pharmaceutical industry as a precursor reagent in the synthesis of a number of synthetic anticoagulant pharmaceuticals similar to dicoumarol, the notable ones being warfarin (brand name Coumadin) and some even more potent rodenticides that work by the same anticoagulant mechanism. Coumarins are a type of vitamin K antagonists.

Pharmaceutical coumarins were all developed from the study of sweet clover disease. Coumarin is found naturally in many plants, notably in high concentration in the tonka bean.

Coumarin and its derivatives are studied by several authors. Experimental Spectroscopic (FT-IR, FT-Raman, NMR) and DFT Studies of 7-methoxy-4-bromomethylcoumarin are studied by N. Prabavathi et.al [1]. FTIR,

FT-Raman, FT-NMR and quantum chemical investigations of 3-acetylcoumarin were investigated by V. Arjunan et.al [2]. Molecular structure, vibrational spectroscopic studies and natural bond orbital analysis of 7-amino-4-trifluoromethyl coumarin was reported by M.K. Subramanian et.al [3]. Scaled Quantum Chemical Calculations and FT-IR, FT- Raman Spectral Analysis of 4-Hydroxy-3-Nitrocoumarin was carried out by M.Sivasubramanian [4]. FT-IR, FT-Raman and UV–Vis spectra and DFT calculations of 3-cyano-4-methylcoumarin are studied earlier by N. Udaya Sri et.al[5].

In the present work, harmonic-vibrational frequencies are calculated for 4-chloro-3-formyl-6-methylcourmarin (4C3F6MC) using B3LYP with 6-31G(d, p) and 6-311++G(d,p) methods. The calculated spectra of the compound are compared to that of experimentally observed FT-IR and FT-Raman spectra. The redistribution of electron density (ED) in various bonding and antibonding orbitals and E(2) energies have been calculated by natural bond orbital (NBO) analysis by DFT method to give clear evidence of stabilization originating from the hyper conjugation of various intramolecular interactions. The HOMO and LUMO analysis have been used to elucidate information regarding ionization potential (IP), electron affinity (EA), electronegativity (χ), electrophilicity index (ω), hardness (η), chemical potential (μ),softness (S) and are all correlated. These are confirming the charge transfer within the molecule and also molecular electrostatic potential (MEP) contour map show the various electrophilic region of the title molecule. However, molecular hyperpolarizability is also calculated by DFT method. Finally, the correlations between thermodynamic properties with various temperatures are reported.

Experimental

The compound 4-chloro-3-formyl-6-methylcourmarin (4C3F6MC) was purchased from Sigma Aldrich chemicals, USA in the solid form and used as such to record the FTIR and FT-Raman spectra. The FTIR spectrum was recorded by KBr pellet method on a Bruker IFS 66 V spectrometer equipped with a Globar source, Ge/KBr beam splitter, and a TGS detector in the range of 4000–400 cm^{-1}. The spectral resolution was 2 cm^{-1}. The FT-Raman spectrum was also recorded in the range 3500–100 cm^{-1} using the same instrument with FRA106 Raman module equipped with Nd:YAG laser source operating at 1.064 μm with 200mW power. A liquid nitrogen cooled-Ge detector was used. The frequencies of all sharp bands are accurate to 2 cm^{-1}.

Computational details

Density functional theory(DFT) computations of 4C3F6MC were performed by using Gaussian 03 program package [6] at the Becke–Lee–Yang–Parr hybrid exchange–correlation three-parameter functional (B3LYP) level with standard 6-31G(d,p) and 6-31++G (d,p) basis sets to derive the complete geometry optimization. All the optimized geometry corresponding to minimum on the potential energy surface has been obtained by solving self-consistent field equation iteratively. The calculated harmonic vibrational wavenumbers have been analytically calculated by taking second order derivative of energy using the similar level of theory. The calculated wavenumbers were scaled with scaling factors. The vibrational modes were assigned on the basis of PED analysis using VEDA 4 program [7].

The Raman scattering activities (Si) calculated by Gaussian 03W program were suitably converted to relative Raman intensities (Ii) using the following relationship derived from the basic theory of Raman scattering [8].

$$I_i = \frac{f(\nu_o - \nu_i)^4 S_i}{\nu_i[1-\exp(-hc\nu_i/k_bT)]}$$

where ν_o is the exciting frequency in cm^{-1}, ν_i the vibrational wave number of the i^{th} normal mode, h, c and k_b are the fundamental constants and f is a suitably chosen common normalisation factor for all the peak intensities.

Result and Discussion

Molecular geometry

The molecular structure of 4C3F6MC is shown in Fig. 1. The calculated optimized geometrical parameters obtained in this study for 4C3F6MC are presented in Table 1. From the experimental values of literature [9], C-C single bond length is 1.5037 Å, C–H single bond length is 1.0853 Å and C–Cl bond length is 1.827 Å for chlorotoluene. The C–Cl bond length (Cl atom of –CH2Cl group) is 1.821 Å in the earlier work done by Durig et.al. [10] and the bond distance is more consistent with the results from the electron diffraction study [11]. From the literature [12] C–C bond length increased from 1.386 to 1.414 Å, while the C–H bond length varies from 1.073 to 1.076 Å for chlorotoluene. For 4C3F6MC the C–C and C–H bond length varies from1.369 to 1.509 Å and 1.083 to 1.105 Å, respectively. Taking account of the effect of conjugation, the calculated values of 4C3F6MC is in reasonable agreement with the above mentioned experimental data. Electron with drawing nature of Chlorine increases the double bond character by redistributing the π-electrons in a more highly shared arrangement. This will increase the bond length of chlorine as compared to other bond lengths. Hence for 4C3F6MC, C–Cl bond length is the maximum (1.757 Å).

Vibrational assignment

The title compound 4C3F6MC was belong to C1 symmetry point group. The theoretically calculated DFT force fields were transformed to this latter set of vibrational coordinates and used in all subsequent calculations. The total energy distribution (TED) for each normal mode among the symmetry coordinates of the molecules was calculated. A complete assignment of the fundamentals was proposed based on the calculated TED values, infrared band intensities and Raman activities. The scaled B3LYP/6-31G (d,p) and 6-311++G(d,p) vibrational frequencies are generally larger than the experimental value. This is partly due to the neglect of anharmonicity and partly due to approximate nature of the quantum mechanical methods. However, for reliable information on the vibrational properties the use of selective scaling is necessary. The calculated wavenumbers are scaled using the set of transferable scale factors recommended by Rauhut and Pulay [13]. The detailed vibrational assignments of fundamental modes of the title molecule along with the calculated IR, Raman intensities and normal mode descriptions were reported in Table 2. For visual comparison, the observed and simulated FTIR and FT-Raman spectra were presented in Figs. 2 and 3 respectively.

C–H vibrations

Aromatic compounds commonly exhibit multiple weak bands in the region 3100–

3000 cm^{-1} due to aromatic C–H stretching vibrations. The bands due to C–H in-plane ring bending vibrations, interacting somewhat with C–C stretching vibrations, are observed as a number of medium–weak intensity sharp bands in the region 1300–1000 cm^{-1}. The C–H out-of-plane bending vibrations are strongly coupled vibration and occur in the region 900–667 cm^{-1} [14]. In this work, the FT-IR bands at 3102, 3100, 3069 and 3018 cm^{-1} and Raman bands at 3103, 3101, 3069 and 3018 cm^{-1} are assigned to C–H stretching vibrations. The peaks at 1267 1124 and 1031 cm^{-1} in FT-IR and 1265, 1125 and 1032 cm^{-1} in Raman are assigned to C–H in-plane bending vibrations. The vibrations due to C–H stretching and in-plane bending vibrations are good agreement with the theoretically computed values by B3LYP/6-31G(d,p) and 6-311++G(d,p) methods.

C–Cl vibrations

The vibrations belonging to the bond between the ring and halogen atoms are worth to discuss here since mixing of vibrations are possible due to the lowering of molecular symmetry and the presence of heavy atoms on periphery of the molecule [15,16]. The X-sensitive C–Cl stretching band is expected around 1105–1045 cm^{-1} [17]. As revealed by the PED, the C–Cl stretching vibration was observed at 838 cm^{-1} in the FT-IR and at 837cm^{-1} in Raman spectrum. The theoretically calculated value at 837 cm^{-1} by DFT method show very good correlation with our experimental observation. In the present work, the FT-Raman band observed at 288 and 222 cm^{-1} was assigned to C-Cl in-plane bending vibration which was in good agreement with the scaled value. The C-Cl out-of-plane bending vibration was observed at 515 and 606 cm^{-1} in FT-IR and FT-R spectrum and correlates good with the calculated values. For 2-amino-5-chlorobenzonitrile [18] molecule the strong FT-IR band at 900 cm^{-1} with 86% PED was assigned to C–Cl stretching mode.

Carbon vibrations

The carbon–carbon stretching modes of the pyridine ring appear in the region 1650–1200 cm^{-1} are determined not so much by the nature of the substituents but by the form of substitution around the ring [19,20]. In 4C3F6MC under C1 symmetry the carbon–carbon stretching bands in the infrared spectrum appeared at 1602, 1522 and 1338 cm^{-1}. The bands observed at 1603, 1528 and 1331 cm^{-1} in 4C3F6MC corresponds to Raman bands assigned to the ring carbon–carbon stretching vibrations. All other observed skeletal C–C stretching, CCC in-plane and out of plane bending vibrations of the compounds are completely assigned and are presented in Table 2. The CCC in-plane bending vibrations of 4C3F6MC were observed in the infrared spectrum at 1231,889 and 627 cm^{-1} and in the Raman spectrum at 1231, 889 and 625 cm^{-1}. At lower frequencies the assignments become more complex since the bands are no longer corresponds to pure motions and also not sensitive to position of substitution.

Methyl group vibrations

The compound under consideration 4C3F6MC possess a CH3 group in the side substitution chain. There are nine fundamentals one can expect to a CH3 group, namely the symmetrical stretching in CH3 (CH3 sym. stretch) and asymmetrical stretching (in plane hydrogen stretching mode); the symmetrical (CH3 sym. deform) and asymmetrical (CH3 asym. deform) deformation modes; inplane rocking, out-of-plane rocking, twisting and bending modes

[21]. Each methyl group has three stretching vibrations, one being symmetric and other two asymmetric. The frequencies of asymmetric vibrations are higher than the symmetric one [22]. The experimentally observed values at 2874cm^{-1} in FTIR and FT-Raman spectrum were assigned for CH3 symmetric stretching and at 2930 and 2979 cm^{-1} in IR and 2932, 2986 cm^{-1} in Raman spectrum for CH3 asymmetric stretching shows an excellent agreement with the range allotted by Dudley et. al. [23]. The torsion vibrations are not observed in the FTIR and FT Raman spectrum because these appear at very low frequency. The observations in 4C3F6MC are in agreement with theoretical results of similar compounds [24].

C-O vibrations

Ketones, aldehydes, carboxylic acids, carboxylic esters, lactones, acid halides, anhydrides, and lactams show a strong C=O stretching absorption band in the region of 1870-1540 cm^{-1}. Within its given range, the position of the C=O stretching band is determined by the following factors (1) physical state (2) electronic and mass effects of neighbouring substituents (3) conjugation (4) hydrogen bonding and (5) ring strain. Consideration of these factors leads to a considerable amount of information about the environment of the C=O group. Probably the direction of the shift depends on whether the inductive effect (or) resonance effect predominates [14]. In the present work, the carbonyl stretching frequency is observed in the high frequency region as a very strong band at 1800cm^{-1} and 1717cm^{-1} in IR and at 1803 and 1712cm^{-1} in Raman spectra. The wavenumbers observed at 585, 512 cm^{-1} in FT-IR and at 583, 511cm^{-1} in FT-Raman spectra are assigned to C-O in-plane bending. The out-of-plane bending of 4C3F6MC is observed at 722, 705cm^{-1} in FT-IR spectra and at 723, 706cm^{-1} in Raman spectra.

Other Molecular properties

Molecular electrostatic potential (MEP)

Molecular electrostatic potential (MEP) generally present in the space around the molecule by the charge distribution is very useful in understanding the sites of electrophilic attacks and nucleophilic reaction for the study of biological recognition process [25] and hydrogen bonding interactions [26–28]. The electrostatic potential V(r) is also well suited for analyzing processes based on the ‘‘recognition’’of one molecule by another, as in drug-receptor, and enzyme–substrate interactions, because it is through their potentials that the two species first ‘‘see’’ each other [29,30]. To predict reactive sites of electrophilic and nucleophilic attacks for the investigated molecule, MEP at the B3LYP/SDD optimized geometry was calculated. The different values of the electrostatic potential at the surface are represented by different colors. Potential increases in the order red < orange < yellow < green < blue. Blue indicates strongest attraction and red indicates the strongest repulsion. The negative (red and yellow) regions of MEP were related to electrophilic reactivity and the positive (blue) regions to nucleophilic reactivity (Fig. 4). As can be seen from the MEP map of the title molecule, while regions having the negative potential are over the electronegative atoms (oxygen), the regions having the positive potential are over the hydrogen atoms.

NBO analysis

Natural bond analysis gives the accurate possible natural Lewis structure picture of ϕ because all orbitals are mathematically chosen to include the highest possible percentage of the electron density. Interaction between both filled and virtual

orbital spaces information correctly explained by the NBO analysis could enhance the analysis of intra- and intermolecular interactions. The second order Fock matrix was carried out to evaluate donor (i) and acceptor (j) i.e. donor level bonds to acceptor level bonds interaction in the NBO analysis [31]. The result of interaction is a loss of occupancy from the concentrations of electron NBO of the idealized Lewis structure into an empty non-Lewise orbital. For each donor(i) and acceptor(j), the stabilization energy E(2) associated with the delocalization i→j is estimated as $E^{(2)} = \Delta E_{ij} = q_i \frac{F(i,j)^2}{\varepsilon_j - \varepsilon_i}$ where q_i is the donor orbital occupancy, ε_i and ε_j are diagonal elements and F (i, j) is the off diagonal NBO Fock matrix element.

Natural bond orbital analysis is used for investigating charge transfer or conjugative interaction in the molecular systems. Some electron donor orbital, acceptor orbital and the interacting stabilization energy results from the second-order micro-disturbance theory are reported [32,33]. The larger E(2) value the more intensive is the interaction between electron donors and acceptors, i.e. the more donation tendency from electron donors to electron acceptors and the greater the extent of conjugation of the whole system [34]. Delocalization of electron density between occupied Lewis-type (bond or lone pair) NBO orbitals and formally unoccupied (antibond or Rydgberg) non-Lewis NBO orbitals correspond to a stabilization donor–acceptor interaction. NBO analysis has been performed on the 4C3F6MC molecule at the DFT/B3LYP/6-31G(d,p) level in order to elucidate the intramolecular interaction within the molecule.

The intramolecular interaction is formed by the orbital overlap between bonding π(C7–C8), π(C9-C10) and antibonding π*(C9–C10), π*(C6–C11) orbital, which results in the intramolecular charge transfer causing stabilization of the system. The second-order perturbation theory of Fock matrix in the NBO analysis shows strong intramolecular hyperconjugative interactions and the results are shown in Table 3. The most important interactions observed are π*(C6-C11)→π*(C7-C8) and π*(C6-C11)→π*(C9-C10) and the corresponding energies are 141.12 and 254.10kJ/mol respectively. This larger energy provides the stabilization to the molecular structure.

Second-order non-linear optical (NLO) properties

The first order hyperpolarizabilities (β_0) of this novel molecular system, and related properties (β, α_0 and Δα) of 4C3F6MC were calculated using B3LYP/6-31 G (d,p) and 6-311++G(d,p) basis sets, based on the finite-field approach. In the presence of an applied electric field, the energy of a system is a function of the electric field. Polarizabilities and hyperpolarizabilities characterize the response of a system in an applied electric field [35]. They determine not only the strength of molecular interactions (long-range inter induction, dispersion force, etc.) as well as the cross sections of different scattering and collision process but also the nonlinear optical properties (NLO) of the system [36,37]. First order hyperpolarizability is a third rank tensor that can be described by 3 × 3 × 3 matrix. The 27 components of the 3D matrix can be reduced to 10 components due to the Kleinman symmetry [38]. It can be given in the lower tetrahedral format. It is obvious that the lower part of the 3 × 3 × 3 matrices is a tetrahedral. The components of β are defined as the coefficients in the Taylor series expansion of the energy in the external electric field. When the external

electric field is weak and homogeneous, this expansion becomes:

$$E = E^0 - \mu_\alpha F_\alpha - \frac{1}{2}\alpha_{\alpha\beta}F_\alpha F_\beta - \frac{1}{6}\beta_{\alpha\beta\gamma}F_\alpha F_\beta F_\gamma + \cdots$$

where E^0 is the energy of the unperturbed molecules, F_α is the field at the origin μ_α, $\alpha_{\alpha\beta}$ and $\beta_{\alpha\beta\gamma}$ are the components of dipole moments, polarizability and the first order hyperpolarizabilities respectively. The total static dipole moment μ the mean polarizability α_0 the anisotropy of the polarizability $\Delta\alpha$ and the mean first order hyper-polarizability β_0, using the x, y and z components are defined as: [38,39]. The total static dipole moment is

$$\mu = (\mu^2{}_x + \mu^2{}_y + \mu^2{}_z)^{1/2}$$

The isotropic polarizability is

$$\alpha_0 = \frac{\alpha_{xx}+\alpha_{yy}+\alpha_{zz}}{3}$$

The polarizability anisotropy invariant is

$$\Delta\alpha = 2^{-\frac{1}{2}}[(\alpha_{xx}-\alpha_{yy})^2+(\alpha_{yy}-\alpha_{zz})^2+(\alpha_{zz}-\alpha_{xx})^2+6\alpha^2_{xx}]^{\frac{1}{2}}$$

and the average hyperpolarizability is

$$\beta_0 = (\beta^2{}_x + \beta^2{}_y + \beta^2{}_z)^{1/2}$$

and

$$\beta_x = \beta_{xxx} + \beta_{xyy} + \beta_{xzz}$$
$$\beta_y = \beta_{yyy} + \beta_{xxy} + \beta_{yzz}$$
$$\beta_z = \beta_{zzz} + \beta_{xxz} + \beta_{yyz}$$

The total static dipole moment, polarizabilities and first order hyper-polarizabilities of 4C3F6MC were calculated. Table 4 lists the values of the electric dipole moment (Debye) and dipole moment components, polarizabilities and hyperpolarizabilities of the 4C3F6MC. In addition to the isotropic polarizabilities the polarizabilities anisotropy invariant were also calculated. The polarizabilities and first order hyperpolarizabilities of 4C3F6MC are 2.101×10^{-23}esu, 2.386×10^{-23}esu and 6.958×10^{-30}, 7.257×10^{-30} esu by B3LYP/6-31G(d,p) and 6-311++G (d,p) levels, which are comparable with the reported values of similar derivatives [39,40]. We conclude that the title compound is an attractive object for future studies of nonlinear optical properties.

Mulliken population analysis

The natural population analysis of 4C3F6MC is obtained by Mulliken [41] population analysis with B3LYP level using 6-31G(d,p) and 6-311++G(d,p)basis sets. Mulliken population analysis graph of 4C3F6MC is shown in Fig.5. Mulliken atomic charge calculation has an important role in the application of quantum chemical calculation to molecular system because of atomic charge effect, dipole moment, molecular polarizability, electronic structure and a lot of properties of molecular systems. Mulliken atomic charges calculated at the B3LYP/6-31G(d,p) and 6-311++G(d,p) are collected in Table.5.

It is worthy to mention that C2,C6,C8,C11,C13,Cl15 and all hydrogen atoms exhibit positive charges, while O1,O3,O14, C4,C5,C7,C9,C10 and C12 atoms exhibit negative charges. The O1 atom has a maximum negative charge value of about (-0.513725) and C2 atom has a maximum positive charge value of about (0.580030) of the title molecule 4C3F6MC calculated using B3LYP/6-31G(d,p) and 6-311++G(d,p) level of theory.

UV-Visible spectral analysis

Time-dependent density functional theory(TD-DFT) calculation has been performed for 4C3F6MC on the basis of fully optimized ground state structure to investigate the electronic absorption properties. The λ_{max} values are obtained from the UV-Vis spectra analyzed theoretically with B3LYP/6-31G(d,p) basis set. The calculated visible absorption maxima which are a function of electron availability theoretical electronic excitation energies are all tabulated in Table.6. The experimental and theoretically predicted UV-Vis spectra are visualized in Fig. 6. It can be seen from the Table 6, the calculated absorption maxima values for 4C3F6MC have been found to be 363.02(gas phase) and 369.11(ethanol). The experimental values are observed at 361 respectively due to $\pi \rightarrow \pi^*$ transition.

Frontier molecular orbital analysis

Both the highest occupied molecular orbital (HOMO) and lowest unoccupied molecular orbital (LUMO) are the main orbitals that take part in chemical stability [42]. The HOMO represents the ability to donate an electron, LUMO as an electron acceptor represents the ability to obtain an electron. The HOMO and LUMO energy calculated by B3LYP/6-31G (d,p) and 6-311++G(d,p) methods is shown in Table 7. This electronic absorption corresponds to the transition from the ground to the first excited state and is mainly described by one electron excitation from the highest occupied molecular orbital (HOMO) to the lowest unoccupied molecular orbital (LUMO). The HOMO is located over the C–Cl and C=O group. And the LUMO is located over the C-C and C-H group, HOMO→LUMO transition implies an electron density transfer to ring from C–Cl and C=O bond. Moreover, these orbitals significantly overlap in their position for 4C3F6MC. The atomic orbital compositions of the frontier molecular orbital are sketched in Fig. 7.

HOMO energy (B3LYP) = −6.81378eV
LUMO energy (B3LYP) = −2.84796 eV
HOMO − LUMO energy gap (B3LYP) = 3.96582 eV

The HOMO and LUMO energy gap explains the eventual charge transfer interactions taking place within the molecule.

Global and local reactivity descriptors

The energy gap between HOMO and LUMO is a critical parameter to determine the molecular electrical transport properties. By using HOMO and LUMO energy values for a molecule, the global chemical reactivity descriptors of molecules such as hardness, chemical potential, softness, electronegativity and electrophilicity index as well as local reactivity have been defined [43-47]. Pauling introduced the concept of electronegativity as the power of an atom in a molecule to attract electrons to it. Hardness (η), chemical potential (μ) and electronegativity (χ) and softness(S) are defined as follows.

$$\eta = \frac{1}{2}\left(\frac{\partial_2 E}{\partial N_2}\right)V(r) = \frac{1}{2}\left(\frac{\partial \mu}{\partial N}\right)V(r)$$

$$\mu = \left(\frac{\partial E}{\partial N}\right) V(r)$$

$$\chi = -\mu = -\left(\frac{\partial E}{\partial N}\right) V(r)$$

where E and V(r) are the electronic energy and the external potential of an N-electron system respectively. Softness is a property of molecule that measures the extent of chemical reactivity. It is the reciprocal of hardness.

Table.1 Optimized geometrical parameters of 4C3F6MC

Bond length(Å)	B3LYP		Bond angle(°)	B3LYP	
	6-31G(d,p)	6-311++G(d,p)		6-31G(d,p)	6-311++G(d,p)
O1-C2	1.402	1.403	C2-O1-C11	123.3	123.4
O1-C11	1.355	1.353	O1-C2-O3	116.9	116.9
C2-O3	1.199	1.193	O1-C2-C4	116.1	116.0
C2-C4	1.478	1.477	O3-C2-C4	126.9	127.0
C4-C5	1.369	1.368	C2-C4-C5	119.3	119.3
C4-C13	1.491	1.492	C2-C4-C13	118.2	118.5
C5-C6	1.442	1.440	C5-C4-C13	122.3	122.0
C5-Cl15	1.757	1.755	C4-C5-C6	122.7	122.8
C6-C7	1.411	1.411	C4-C5-Cl15	120.7	120.7
C6-C11	1.408	1.405	C6-C5-Cl15	116.5	116.4
C7-C8	1.387	1.384	C5-C6-C7	125.3	125.2
C7-H16	1.083	1.081	C5-C6-C11	116.1	116.2
C8-C9	1.411	1.409	C7-C6-C11	118.4	118.4
C8-C12	1.509	1.508	C6-C7-C8	121.6	121.6
C9-C10	1.385	1.383	C6-C7-H16	118.7	118.6
C9-H17	1.086	1.085	C8-C7-H16	119.6	119.6
C10-C11	1.397	1.395	C7-C8-C9	118.2	118.1
C10-H18	1.084	1.082	C7-C8-C12	121.3	121.4
C12-H19	1.095	1.094	C9-C8-C12	120.3	120.3
C12-H20	1.095	1.094	C8-C9-C10	121.6	121.6
C12-H21	1.092	1.091	C8-C9-H17	119.2	119.2
C13-O14	1.211	1.206	C10-C9-H17	119.0	119.0
C13-H22	1.105	1.102	C9-C10-C11	119.3	119.3
			C9-C10-H18	121.9	121.9
			C11-C10-H18	118.6	118.7
			O1-C11-C6	122.1	122.0
			O1-C11-C10	117.1	117.2
			C6-C11-C10	120.7	120.7
			C8-C12-H19	111.2	111.1
			C8-C12-H20	111.2	111.1
			C8-C12-H21	111.4	111.3
			H19-C12-H20	107.1	107.2
			H19-C12-H21	107.7	107.8
			H20-C12-H21	107.8	107.8
			C4-C13-O14	125.2	125.5
			C4-C13-H22	113.8	113.7
			O14-C13-H22	120.8	120.6

Table.2 Vibrational Assignments of 4C3F6MC

Mode No.	Experimental		Calculated B3LYP		Vibrational Assignments + PED(%)
	FT-IR υcm^{-1}	FT-R υcm^{-1}	6-31G(d,p) Scaled υcm^{-1}	6-311++G(d,p) Scaled υcm^{-1}	
1	3102	3103	3106	3103	υCH(89)
2	3100	3101	3103	3101	υCH(93)
3	3069	3069	3070	3067	υCH(96)
4	3018	3018	3018	3010	υCH(91)
5	2979	2986	2986	2978	υCH_3(96)
6	2930	2932	2931	2930	υCH_3(99)
7	2874	2874	2874	2877	υCH_3(94)
8	1800	1803	1803	1786	υOC(89)
9	1717	1712	1717	1707	υOC(94)
10	1602	1603	1609	1602	υCC(51)+βCCC(10)
11	1565	1566	1567	1561	υCC(39)
12	1522	1528	1528	1518	υCC(48)
13	1463	1461	1467	1461	υCC(14) +βHCC(32)
14	1453	1454	1455	1450	βCH_3 (62)
15	1440	1441	1442	1439	τHCCC(11)+βHCH(81)
16	1408	1408	1408	1403	βHCO(50)
17	1381	1385	1385	1380	υCC(10) +βHCO(41)
18	1376	1377	1379	1375	βCH_3(91)
19	1338	1331	1339	1330	υCC(55)
20	1281	1277	1282	1277	υCC (10)+ βHCC(10)+ βCCC(18)
21	1267	1265	1267	1264	υOC(14)+βHCC(52)
22	1231	1231	1234	1231	υOC(21)+βCCC(26) +βHCC(18)
23	1196	1204	1202	1195	υCC(41)+βCCC(11)
24	1144	1144	1144	1141	υCC(45)+ βHCC(15)
25	1124	1125	1124	1126	υCC(15)+ βHCC(61)
26	1031	1032	1030	1032	βHCH(26)+ τHCCC(55)
27	1000	1001	1000	1000	υCC(14)+ βHCH(10)+τHCCC(45)
28	974	974	975	974	υCC(11)+ υOC(50)
29	960	959	962	959	τHCCC(79)+τOCCC(12)
30	944	945	944	951	υCC(19)+ βCCC(14)
31	942	943	943	943	τHCCC(80)
32	889	889	889	889	βCCC(25)
33	871	870	870	873	τHCCC(71)
34	838	837	837	837	υCC(11)+νClC(22)
35	813	814	813	814	τHCCC(77)+γOCCC(10)
36	746	745	743	745	υCC(28)+βCCC(13)
37	722	723	722	721	τCCCC(25)+γOCOC(20)+ γCCCC(21)
38	705	706	705	710	γOCOC(55)+ γOCCC(11)
39	698	698	698	697	υCC(10)+βCCC(21)+ βOCC(20)
40	627	625	625	628	βCCC(38)
41	606	606	605	607	τCCCC(13)+γClCCC(34)
42	585	583	581	583	υOC(11)+υCC(11)+βCOC(10)+βOCO(18)
43	515	515	517	515	τCCCC(14)+γClCCC(14)+ γOCCC(23)+γCCCC(15)
44	512	511	509	511	βCOC(14)+βOCO(20)+ βOCC(31)
45	427	428	427	425	τCCCC(53)+γCCCC(12)
46	422	421	421	423	βCOC(13)+βCCC(29)

47	399	397	395	397	υClC(29)+βCCC(24)
48	-	351	350	351	υCC(39)+βCCC(20)
49	-	338	338	333	τCCCC(13)+γCCCC(33)+γOCCC(20)
50	-	328	327	327	νClC(14)+βOCO(11)+βCCC(11)+βOCC(20)
51	-	288	288	288	βCCC(19)+βClCC(38)
52	-	274	273	267	γCCCC(65)
53	-	222	223	221	βOCC(10)+βCCC(45)+βClCC(26)
54	-	172	172	171	βCCC(52)+βClCC(12)
55	-	164	167	164	τCCCC(25)+τCOCC(16)+γCCCC(38)
56	-	126	130	126	τCOCC(25)+γClCCC(16)+γOCCC(12)+γCCCC(24)

υ- stretching; β: in-plane-bending; γ: out-of-plane bending; τ- torsion

Table.3 Second order perturbation theory analysis of Fock matrix in NBO analysis

Donor(i)	Acceptor(j)	E(2)[a] (kJ/mol)	E(j)–E(i)[b] (a.u.)	F(i, j)[c] (a.u.)
π(C7-C8)	π*(C9-C10)	20.31	0.27	0.066
π(C9-C10)	π*(C6-C11)	22.04	0.26	0.070
LP(2) O1	π*(C2-O3)	26.48	0.33	0.084
LP(2) O1	π*(C6-C11)	33.51	0.34	0.100
LP(2) O3	σ*(O1-C2)	44.06	0.46	0.128
LP(2) O3	σ*(C2-C4)	18.08	0.63	0.099
LP(2) O14	σ*(C4-C13)	23.88	0.65	0.112
LP(2) O14	σ*(C13-H22)	19.91	0.66	0.104
π*(C6-C11)	π*(C7-C8)	141.12	0.02	0.075
π*(C6-C11)	π*(C9-C10)	254.10	0.01	0.079

a E(2) means energy of hyper conjugative interaction (stabilization energy).
b Energy difference between donor and acceptor i and j NBO orbitals.
c F(i,j) is the fock matrix element between i and j NBO orbitals

Table.4 NLO properties of 4C3F6MC

Parameters	B3LYP		Parameters	B3LYP	
	6-31G(d,p)	6-311++G(d,p)		6-31G(d,p)	6-311++G(d,p)
μ_x	-7.3513	-7.7866	β_{xxx}	628.082	701.203
μ_y	2.4160	2.8115	β_{xxy}	464.663	513.562
μ_z	0.2553	0.3728	β_{xyy}	93.4923	86.2911
μ_{tot}	7.7423	8.2870	β_{yyy}	-34.8949	-58.7928
α_{xx}	227.603	246.354	β_{xxz}	-0.213052	0.155514
α_{xy}	-3.020	-4.184	β_{xyz}	-0.138576	-0.220017
α_{yy}	145.031	159.693	β_{yyz}	-0.260603	-0.086327
α_{xz}	0.066	0.147	β_{xzz}	-39.2281	-84.9628
α_{yz}	0.011	0.001	β_{yzz}	-1.77008	5.77222
α_{zz}	52.816	77.001	β_{zzz}	0.468595	0.217654
α_{tot} (esu)	2.101×10^{-23}	2.386×10^{-23}	β_{tot}(e.s.u)	6.958×10^{-30}	7.257×10^{-23}
$\Delta\alpha$(esu)	6.258×10^{-23}	6.686×10^{-23}			

Table.5 Mulliken atomic charges of 4C3F6MC

Atoms	B3LYP		Atoms	B3LYP	
	6-31G(d,p)	6-311++G(d,p)		6-31G(d,p)	6-311++G(d,p)
O1	-0.513725	-0.126005	C12	-0.383496	-0.301296
C2	0.580030	0.217886	C13	0.260517	-0.132554
O3	-0.409286	-0.213856	O14	-0.376122	-0.208770
C4	-0.024334	0.824822	Cl15	0.049709	0.802573
C5	-0.158057	-0.365835	H16	0.114592	0.146954
C6	0.133187	0.293226	H17	0.101911	0.179041
C7	-0.174129	-1.294959	H18	0.122953	0.206152
C8	0.121776	0.202243	H19	0.138636	0.172968
C9	-0.112284	-0.320587	H20	0.123416	0.157102
C10	-0.105799	-0.262092	H21	0.119792	0.165625
C11	0.301050	-0.285315	H22	0.089662	0.142676

Table.6 UV-Vis excitation energy(□E) of 4C3F6MC

States	TD-B3LYP/6-31G(d,p)				Expt. λ	Major Contributions
	Gas phase		Ethanol			
	λcal	E(eV)	λcal	E(eV)		
S1	406.55	3.0497	407.50	3.0425	398	H−1→LUMO(90%)
S2	363.02	3.4343	369.11	3.3590	361	HOMO→LUMO(86%)
S3	292.23	4.2427	297.94	4.1613	295	H−2→LUMO(75%)

Table.7 Molecular properties of 4C3F6MC

Molecular properties	B3LYP		Molecular properties	B3LYP	
	6-31G(d,p)	6-311++G(d,p)		6-31G(d,p)	6-311++G(d,p)
εHOMO(eV)	-6.81378	-7.14631	Chemical hardness(η)	1.98290	1.96685
εLUMO(eV)	-2.84796	-3.21260	Chemical potential(μ)	-4.83087	-5.17945
ε(H-L) (eV)	-3.96582	-3.93371	Electronegativity(χ)	4.83087	5.17945
Ionization potential(I)	6.81378	7.14631	Electrophilicity index(ω)	11.6686	13.4133
Electron affinity(A)	2.84796	3.21260	Softness(S)	0.504309	0.508425

Fig.1 Optimized Structure of 4C3F6MC

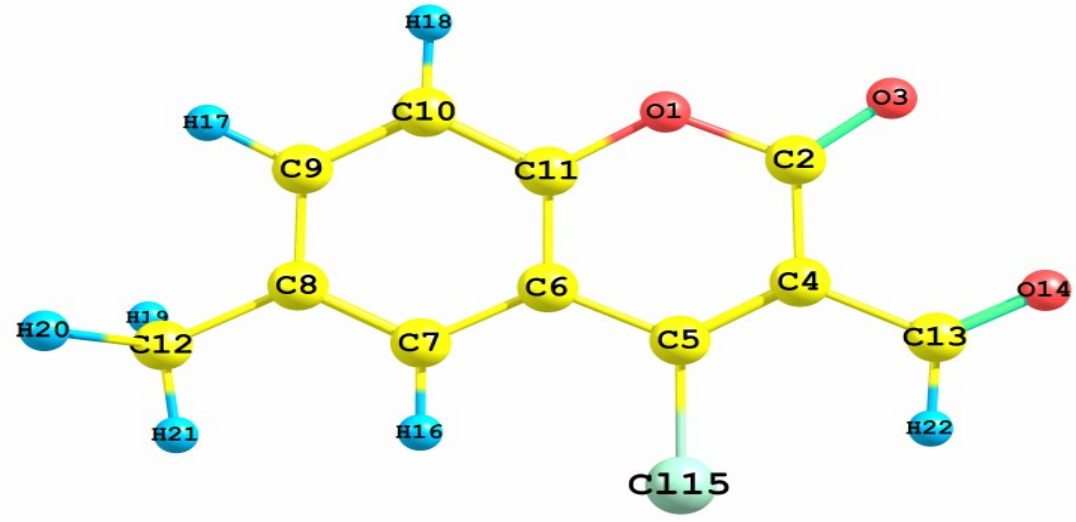

Fig.2 FT-IR spectra of 4C3F6MC

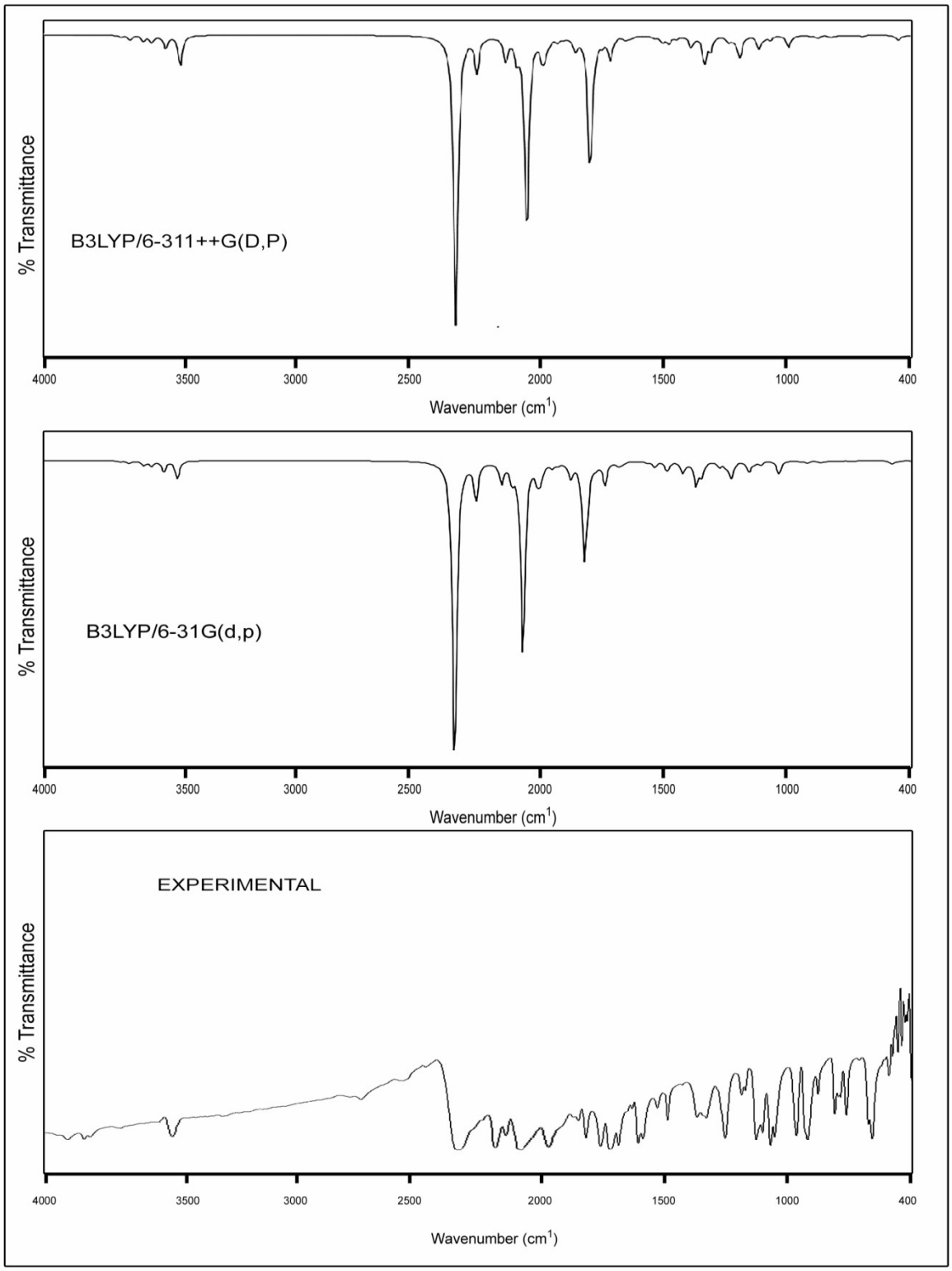

Fig.3 FT-R spectra of 4C3F6MC

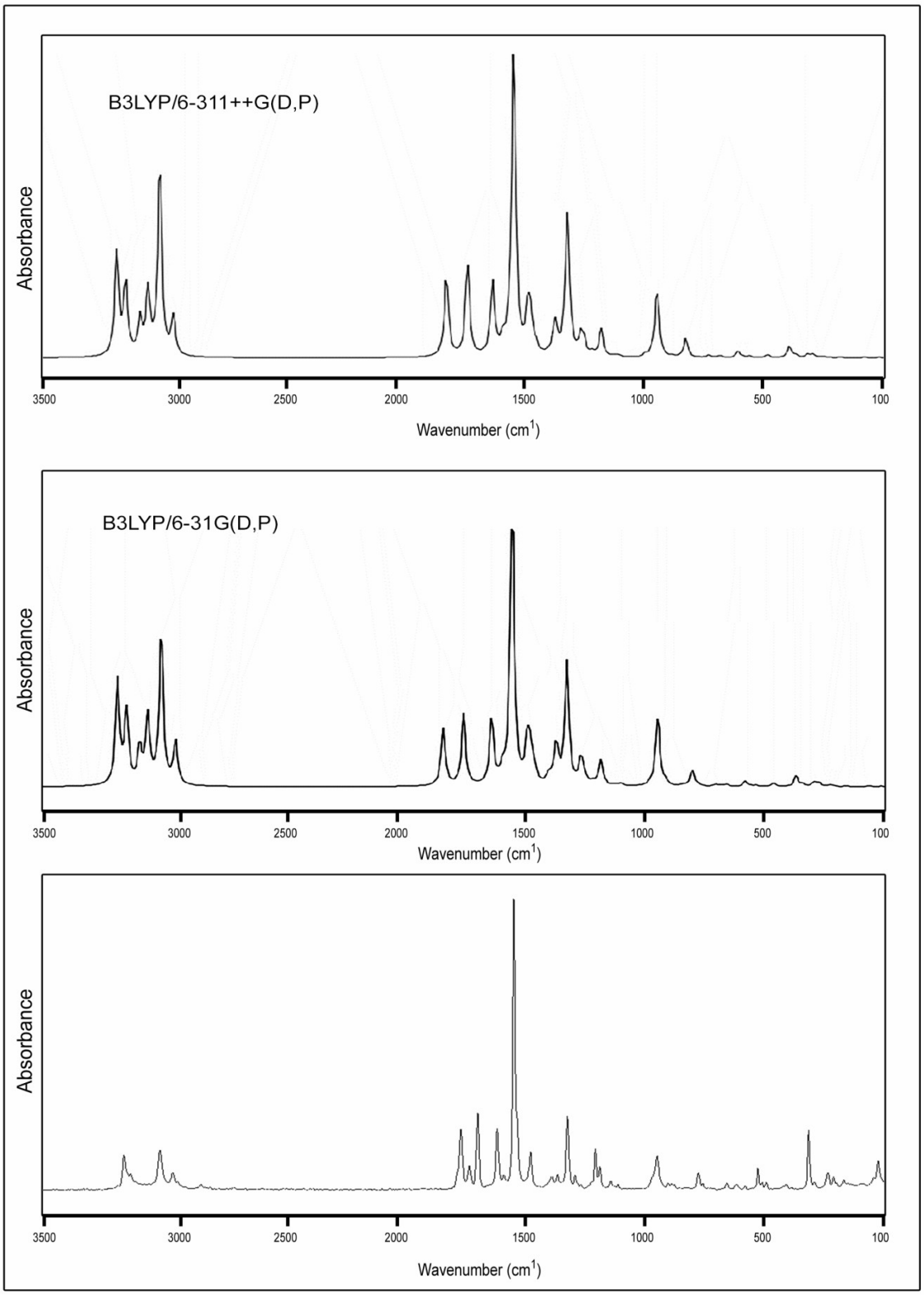

Table.8 Thermodynamic functions of 4C3F6MC

Temperature (T°K)	Entropy(S) (J/mol.k)		Enthalpy($C°_{pm}$)(J/mol.k)		Heat Capacity(ddH)(KJ/mol)	
	B3LYP		B3LYP		B3LYP	
	6-31G(d,p)	6-311++G(d,p)	6-31G(d,p)	6-311++G(d,p)	6-31G(d,p)	6-311++G(d,p)
100.00	332.47	319.25	97.78	90.32	6.53	5.96
200.00	419.06	400.44	158.48	150.45	19.37	18.01
298.15	493.03	471.19	215.20	207.14	37.74	35.59
300.00	494.36	472.48	216.23	208.17	38.14	35.98
400.00	563.83	539.64	267.85	259.91	62.41	59.45
500.00	628.37	602.42	310.67	302.81	91.41	87.66
600.00	688.16	660.78	345.04	337.21	124.26	119.72
700.00	743.50	714.91	372.59	364.74	160.19	154.87
800.00	794.76	765.12	394.89	387.02	198.60	192.50
900.00	842.36	811.79	413.16	405.26	239.03	232.14
1000.00	886.70	855.30	428.30	420.35	281.13	273.45

Fig.4 Molecular electrostatic potential of 4C3F6MC

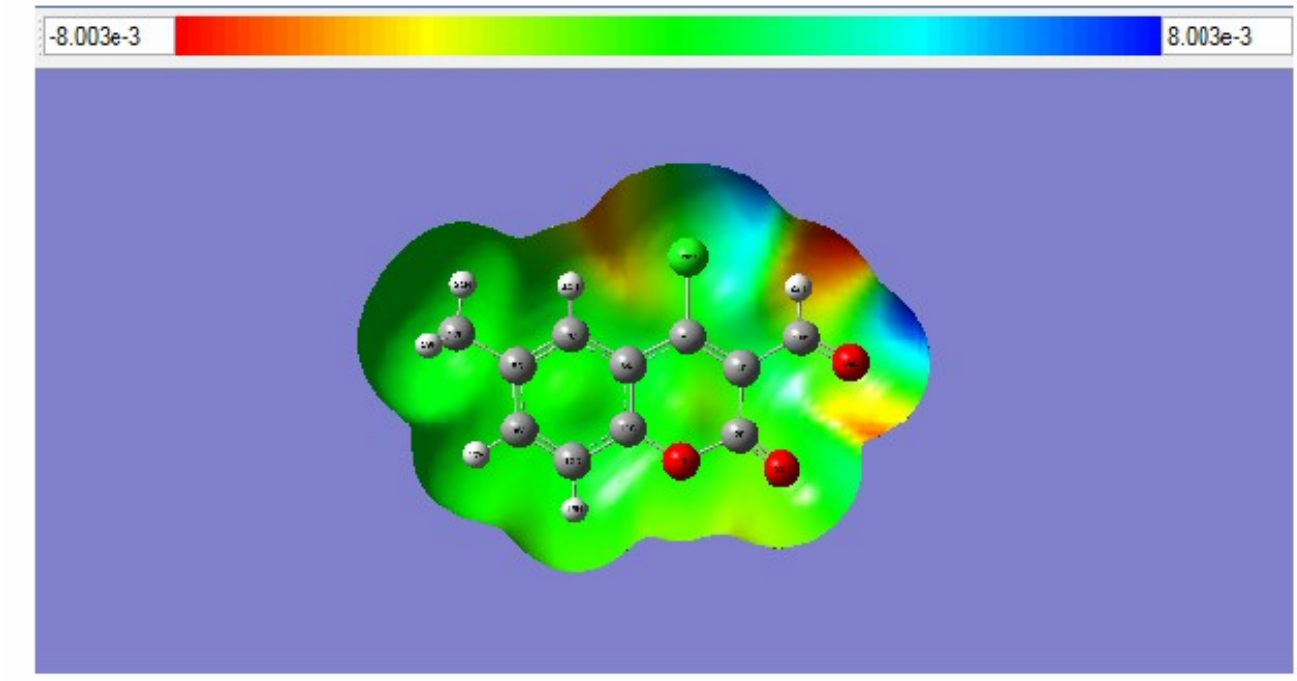

Fig.5 Population charges of 4C3F6MC

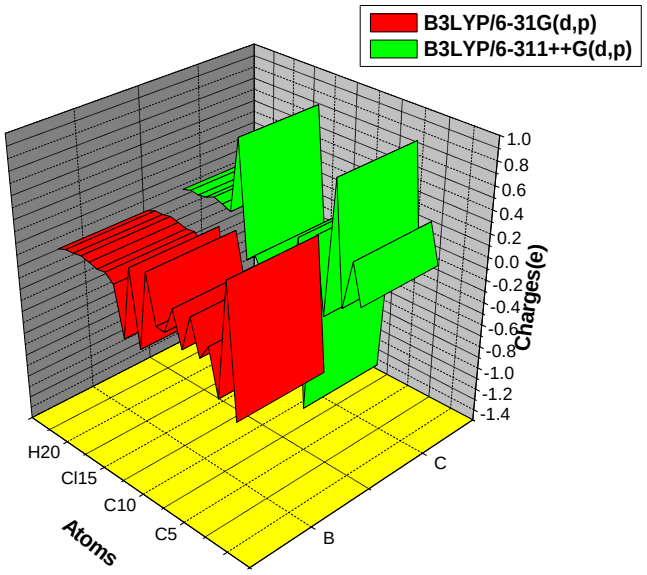

Fig.6 UV-Visible spectrum of 4C3F6MC

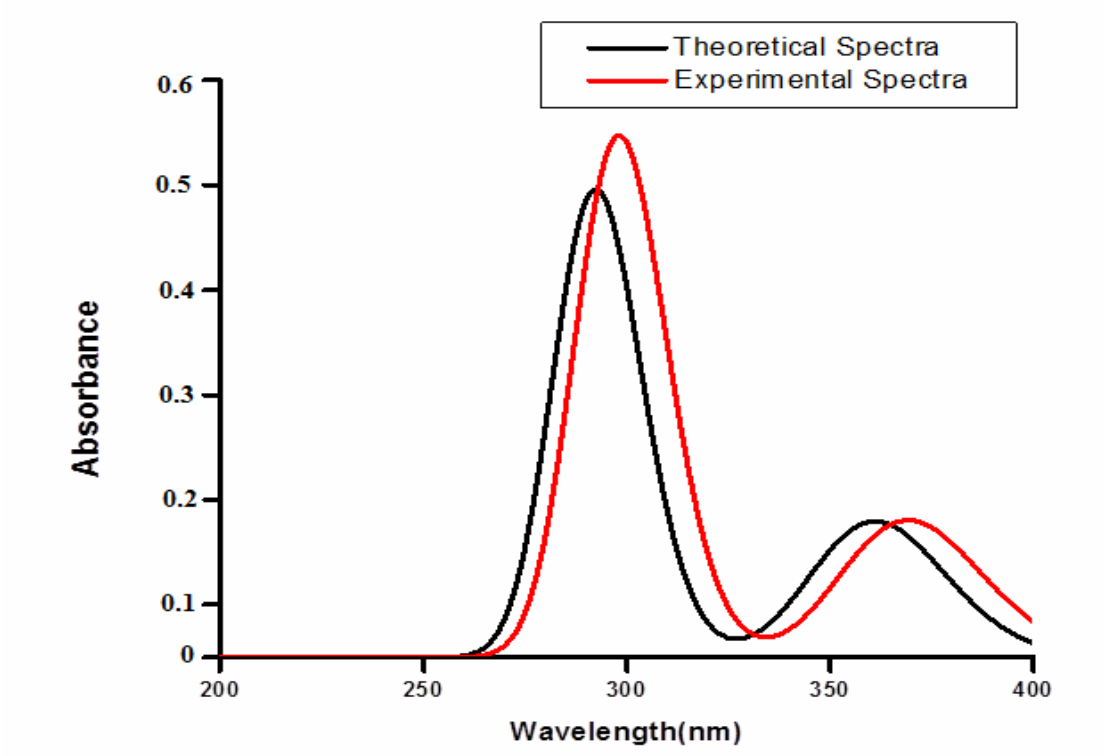

Fig.7 Atomic orbital's of 4C3F6MC

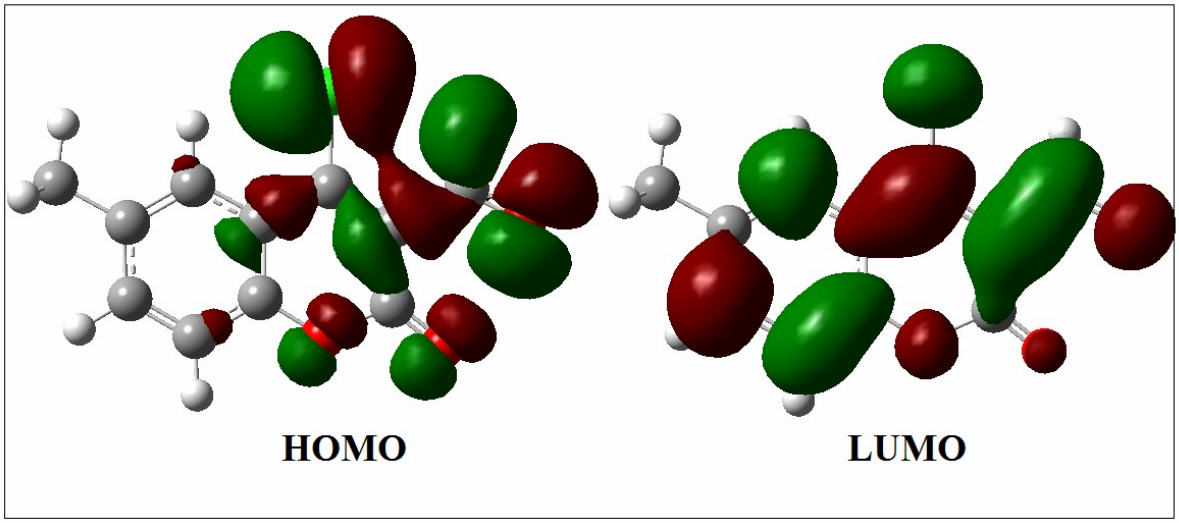

Fig.8 Thermodynamic properties of 4C3F6MC

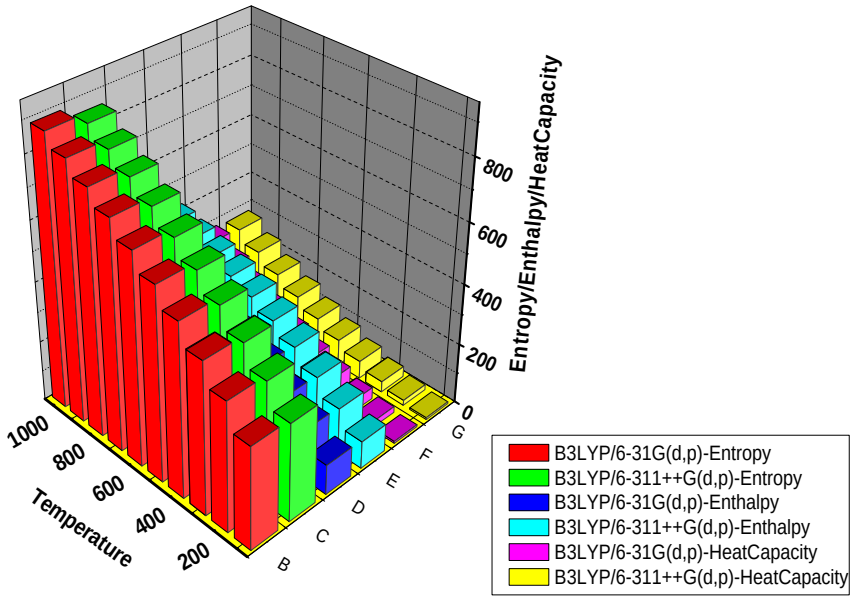

$$S = \frac{1}{\eta}$$

Using Koopman's theorem for closed-shell molecules, η, μ and χ can be defined as

$$\eta = \frac{I-A}{2} \qquad \mu = \frac{-(I+A)}{2} \qquad \chi = \frac{I+A}{2}$$

where I and A are the ionization potential and electron affinity of the molecules respectively. The ionization energy and electron affinity can be expressed through HOMO and LUMO orbital energies as $I = -E_{HOMO}$ and $A = -E_{LUMO}$. The electron affinity refers to the capability of a ligand to accept precisely one electron from a donor. The ionization potential and electron affinity calculated by B3LYP/6-31G (d,p) method for 4C3F6MC is 6.81378eV and 2.84796eV respectively. Considering the chemical hardness, large HOMO–LUMO gap means a hard molecule and small HOMO–LUMO gap means a soft molecule. One can also relate the stability of the molecule to hardness, which means that the molecule with least HOMO–LUMO gap means it is more reactive. Recently Parr et.al. [43] have defined a new descriptor to quantify the global electrophilic power of the molecule as electrophilicity index (ω), which defines a quantitative classification of the global electrophilic nature of a molecule Parr et.al. [43] have proposed electrophilicity index (ω) as a measure of energy lowering due to maximal electron flow between donor and acceptor. They defined electrophilicity index (ω) as follows:

$$\omega = \frac{\mu^2}{2}$$

Using the above equations, the chemical potential, hardness and electrophilicity index have been calculated for 4C3F6MC and their values are shown in Table 7. The usefulness of this new reactivity quantity has been recently demonstrated in understanding the toxicity of various pollutants in terms of their reactivity and site selectivity [48-50]. The calculated value of electrophilicity index describes the biological activity of 4C3F6MC.

Thermodynamic analysis

The frequency calculations compute the zero point energies, thermal correction to internal energy, enthalpy, Gibbs free energy and entropy as well as the heat capacity for a molecular system. The temperature dependence of the thermodynamic properties such as heat capacity(ddH), entropy (S) and enthalpy change (C) for 4C3F6MC were also determined by B3LYP/6-31G(d,p) and 6-311++G(d,p) methods are listed in Table 8 and shown in the Fig.8. The entropies, heat capacities, and enthalpy changes are increasing with temperature ranging from 100 to 1000 K due to the increase in vibrational intensities with temperature. For the title compound, all thermodynamic parameters have been increased steadily.

Conclusion

The FT-IR and FT-Raman spectral studies and NBO analysis of 4C3F6MC were carried out for the first time. A complete vibrational and molecular structure analysis has been performed based on the quantum mechanical approach by DFT calculations. The difference between the observed and scaled frequency values of most of the fundamentals is small. Therefore the assignment made at DFT/6-31G(d,p) and 6-311++G(d,p) medium level of theory almost coincides the values obtained experimentally and few reasonable deviations were observed. The first order hyperpolarizability of the title molecule is calculated to be 6.958×10^{-30} esu which is 18 times greater

than that of urea. Hence, it exhibits good NLO properties. The NBO analysis shows strong intermolecular hyperconjugative interactions of π electron. The strong delocalization of π electron in the molecule leading to a stabilization of the molecule.

References

1.N. Prabavathi N. Senthil Nayaki J. Environ. Nanotechnol. Volume 3, No.2 pp. 108-121

2.V.Arjunan, S.Sakiladevi, M.K. Marchewka, S.Mohan, Spectrochim. Acta 109(2013) 79-89

3.M.K.Subramanian, P.M.Anbarasan,S. Manimegalai PRAMANA-Journal of physics, 74, 5(2010) 845-860

4.M. Sivasubramanian, Int.J Engg. Research & Technology, 1(7), 2012, 278-288

5.N. Udaya Sri, K. Chaitanya, M.V.S. Prasad, V. Veeraiah, A. Veeraiah , Spectrochim. Acta 97(2012) 728-736

6.Gaussian 03, Revision C.02, M.J. Frisch, G.W. Trucks Gaussian, Inc., Wallingford CT, 2004.

7.M.H. Jamróz, Vibrational Energy Distribution Analysis VEDA 4, Warsaw, 2004.

8.T.Gnanasambandan, S.Gunasekaran, S.Seshadri, Spectrochimica Acta A, 112(2013) 52-61.

9.S.H. Vosko, L. Wilk, M. Nusair, Can. J. Phys. 58 (1980) 1200–1211.

10.J.R. Durig, T.G. Costner, T.S. Little, Can. J. Chem. 71 (1993) 1751.

11.Q. Shen, J. Mol. Struct. 75 (1981) 303–310.

12.G.S. Jas, K. Kuezera, Chem. Phys. 214 (1997) 229–241.

13.G.Rahut, P.Pulay, J.Phys. Chem. 99(1995) 3093-3100.

14.M. Silverstein, G. Clayton Basseler, C. Morill, Spectrometric Identification of Organic Compounds, Wiley, New York, 1981.

15.C. Lee, W. Yang, R.G. Parr, Phys. Rev. 37B (1988) 785.

16.B. Lakshmaiah, G. Ramana Rao, J. Raman Spectrosc. 20 (1989) 439.

17.N.B. Colthup, L.H. Daly, S.E. Wiberly, Introduction to Infrared and Raman Spectroscopy, third ed., Academic Press, Boston, 1990.

18.V. Krishnakumar, S. Dheivamalar, Spectrochim. Acta 71A (2008) 465.

19.L.J. Bellamy, The Infrared Spectra of Complex Molecules, third ed., Wiley, NewYork, 1975.

20.G. Varsanyi, Assignments for Vibrational Spectra of Seven Hundred Benzene Derivatives, vol. I, Adam Hilger, London, 1974.

21.T.Gnanasambandan,S. Gunasekaran, S.Seshadri, Spectrochim. Acta 117 (2014) 557-567.

22.M.K. Sharma, K.C. Medhi, Indian J. Phys. 66B (1) (1992) 59–64.

23.N.B. Dudley, H. Williams, Ian Fleming, Spectroscopic Methods in Organic Chemistry, Tata McGraw-Hill, UK, 1988.

24.B.S. Yadav, Israt Ali, Pradeep Kumar, Ptrrti Yadav, Indian J. Pure Appl. Phys. 45 (2007) 979–983.

25.P. Politzer, P.R. Laurence, K. Jayasuriya, Health Persp. 61 (1985) 191–202.

26.P. Politzer, P. Lane, Struct. Chem. 61 (1990) 159–164.

27.E. Scrocco, J. Omasi, Adv. Quantum Chem 103 (1978) 115–193.

28.F.J. Luque, J.M. Lopez, M. Orozco, Theor. Chem. Acc. 103 (2000) 343–345.

29.P. Politzer, J.S. Murray, in: D.L. Beveridge, R. Lavery (Eds.), Theoretical Biochemistry and Molecular Biophysics: A Comprehensive Survey, vol. 2, Protein, Adenine Press, Schenectady, NY, 1991 (Chap. 13).

30.E. Scrocco, J. Tomasi, Top. Curr. Chem. 42 (1973) 95–170.
31.M.Szafran, A.Komasa, E.B.Adamska, J.Mol.Struct.(THEOCHEM) 27,(2007) 101-118.
32.C. James, A. Amal Raj, R. Rehunathan, I. Hubert Joe, V.S. Jayakumar, J. Raman Spectrosc. 37 (2006) 1381.
33.Liu Jun-na, Chen Zhi-rang, Yuan Shen-fang, J. Zhejiag, University Sci. 6B (2005)584.
34.S. Sebastian, N. Sundaraganesan, Spectrochim. Acta 75A (2010) 941.
35.C.R. Zhang, H.S. Chen, G.H. Wang, Chem. Res. Chin. U. 20 (2004) 640–646.
36.Y. Sun, X. Chen, L. Sun, X. Guo, W. Lu, J. Chem. Phys. Lett. 381 (2003) 397–403.
37.O. Christiansen, J. Gauss, J.F. Stanton, J. Chem. Phys. Lett. 305 (1999) 147–155.
38.A. Kleinman, J. Phys. Rev. 126 (1962) 1977–1979.
39.V.B. Jothy, T. Vijayakumar, V.S. Jayakumar, K. Udayalekshmi, K. Ramamoorthy, L.H. Joe, J. Raman Spectrosc. 38 (2007) 1148–1158.
40.O. Prasad, L. Sinha, N. Kumar, J. Atom. Mol. Sci. 1 (2010) 201–214.
41.R.S. Mulliken, J. Chem. Phys. 23 (1995) 1833–1840.
42.T.Gnanasambandan, S.Gunasekaran, S.Seshadri, Spectrochim. Acta A 122 (2014) 542–552.
43.R.G. Parr, L. Szentpaly, S. Liu, J. Am. Chem. Soc. 121 (1999) 1922–1924.
44.P.K. Chattaraj, B. Maiti, U. Sarkar, J. Phys. Chem. A107 (2003) 4973–4975.
45.R.G. Parr, R.A. Donnelly, M. Levy, W.E. Palke, J. Chem. Phys. 68 (1978) 3801–3807.
46.R.G. Parr, R.G. Pearson, J. Am. Chem. Soc. 105 (1983) 7512–7516.
47.R.G. Parr, P.K. Chattraj, J. Am. Chem. Soc. 113 (1991) 1854–1855.
48.R. Parthasarathi, J. Padmanabhan, M. Elango, V. Subramanian, P. Chattaraj, Chem. Phys. Lett. 394 (2004) 225–230.
49.R. Parthasarathi, J. Padmanabhan, V. Subramanian, B. Maiti, P. Chattaraj, Curr.Sci. 86 (2004) 535–542.
50.R. Parthasarathi, J. Padmanabhan, V. Subramanian, U. Sarkar, B. Maiti, P.Chattaraj, Internet Electron. J. Mol. Des. 2 (2003) 798–813.